Materials Today Bio 31 (2025) 101550

Contents lists available at ScienceDirect

Materials Today Bio

journal homepage: www.journals.elsevier.com/materials-today-bio

Dual functional hydrogel of osteoclastic-inhibition and osteogenic-stimulation for osteoporotic bone defect regeneration

Lei Yu [a,c,1], Wentao Wang [a,1], Chang Lv [d,1], Qian Chen [b,1], Peng Yang [a], Zhenrong Qi [b], Haomiao Yu [b], Ruiqi Cao [b], Wenhao Li [a], Yi Qin [a], Gaoran Ge [a], Peilai Liu [c], Lixin Zhu [d,****], Houyi Sun [c,***], Dechun Geng [a,**], Liang Zhang [b,*]

[a] Department of Orthopedics, The First Affiliated Hospital of Soochow University, Orthopedic Institute, Medical College, Soochow University, Suzhou, 215006, Jiangsu, China
[b] Department of Orthopedics, Beijing Friendship Hospital, Capital Medical University, 95 Yongan Road, Xicheng District, Beijing, 100050, China
[c] Department of Orthopedics, Qilu Hospital of Shangdong University, Shandong University, Jinan, 250100, Shandong, China
[d] Department of Spinal Surgery, Orthopedic Medical Center, Zhujiang Hospital, Southern Medical University, Guangzhou, 510280, Guangdong, China

ARTICLE INFO

Keywords:
Osteoporosis
Hydrogel
Alendronate
Osteoclastic differentiation
Osteogenic differentiation
Bone regeneration

ABSTRACT

Osteoporotic bone regeneration poses significant challenges due to the complexity of the condition. Osteoporosis, a degenerative disorder, results from an imbalance in bone homeostasis driven by dysregulation of osteoblast and osteoclast activity. This complicates the treatment of osteoporosis and its related bone injuries in clinical practice. Despite the development of various polymer scaffolds for bone defect repair, achieving effective regeneration in osteoporotic bones—especially when combined with osteoporosis medications—remains difficult. In this study, we designed a drug delivery system composed of mesoporous bioactive glass (MBG) and photo-crosslinked hyaluronic acid methacrylate (HAMA). This system, loaded with the osteogenesis-promoting peptide DWIVA (D5) and the osteoclastogenesis-inhibiting drug alendronate (ALN), is gelled using a light initiator and 405 nm wavelength light. The MBG@D5-Gel complex enables the controlled spatiotemporal release of these agents, markedly enhancing bone regeneration in osteoporotic conditions within ovariectomized rats by inhibiting osteoclastogenesis and bone resorption while promoting osteogenic differentiation and mineralization. This dual-action system synergistically regulates osteoblast and osteoclast activity, optimizing the pathological microenvironment of osteoporosis and facilitating the repair of osteoporotic bone defects. MBG@D5-Gel holds great potential as an effective organic-inorganic hybrid biomimetic implant material for the treatment of osteoporotic bone defects.

1. Introduction

Osteoporosis is a metabolic bone disease characterized by reduced bone mass and disruption of bone microstructure, leading to increased fragility and a higher risk of fractures [1]. This condition predominantly affects postmenopausal women and elderly men, imposing a substantial economic burden on individuals, families, and society [2]. The pathogenesis of osteoporosis is intricately linked to the dysfunction of osteoblasts, osteoclasts, and osteocytes, with an imbalance between bone resorption and formation as its primary pathological mechanism [3,4]. Repairing bone defects under osteoporotic conditions presents a considerable challenge, as reduced bone formation, excessive bone resorption, and changes in both systemic metabolism and the local microenvironment not only complicate the achievement of initial stability but also impede bone integration and regeneration [5–7]. Biomaterials aimed at treating osteoporotic bone defects must inhibit osteoclastogenesis while promoting osteogenesis to improve the pathological microenvironment and maintain bone homeostasis.

* Corresponding author.
** Corresponding author.
*** Corresponding author.
**** Corresponding author.
E-mail addresses: zlx007@smu.edu.cn (L. Zhu), houyi@sdu.edu.cn (H. Sun), szgengdc@suda.edu.cn (D. Geng), zhangliang@ccmu.edu.cn (L. Zhang).
[1] These authors contributed equally to this work.

https://doi.org/10.1016/j.mtbio.2025.101550
Received 5 December 2024; Received in revised form 21 January 2025; Accepted 3 February 2025
Available online 5 February 2025

Alendronate sodium (ALN), a potent bisphosphonate, is widely used to treat osteoporosis due to its strong inhibitory effect on bone resorption [8,9]. However, its clinical application is fraught with challenges, including low bioavailability, poor absorption, and gastrointestinal side effects [10]. Additionally, long-term use of bisphosphonates may lead to nonspecific adverse reactions and reduce the heterogeneity of bone tissue [11]. Bone morphogenetic protein-2 (BMP-2), a member of the TNF-β family, is one of the most potent bioactive factors known to induce osteogenesis. The pentapeptide sequence within the wrist epitope (amino acids 30–34, DWIVA: Asp-Trp-Ile-Val-Ala) binds to BMP type I receptors and induces osteogenic activity [12]. Studies have shown that the D5 peptide can promote the proliferation, differentiation, and extracellular matrix mineralization of osteoblasts *in vitro*. Recent research has increasingly supported the efficacy of combining or sequentially using anti-resorptive agents and osteogenic promoters to achieve positive osteoporosis treatment outcomes. For instance, Allison et al. demonstrated that using parathyroid hormone after alendronate sodium treatment could stimulate new bone formation and increase trabecular thickness and bone volume fraction by affecting the mineralization process [13].

Hydrogels, composed of hydrophilic polymer chains connected by cross-linking points, have garnered significant attention due to their excellent rheological properties, biocompatibility, and capacity for localized drug delivery [14,15]. The biomimetic three-dimensional network structure and hydrophilicity of hydrogels help maintain drug activity, achieve sustained release at the target site, and prolong drug exposure time. Recent studies have found that macromolecular polymers modified with polyphenol-structured drugs can form cross-linked networks through metal ion coordination. While metal-coordinated hydrogels are widely used, the toxicity concerns associated with many metal ions have limited their broader application [16,17]. Advances in the molecular mechanisms of bone regeneration have highlighted the crucial role of calcium ions in osteoblast differentiation, where they stimulate osteogenic activity [18,19]. Additionally, calcium ions are involved in the formation of thrombin complexes, promoting and accelerating blood coagulation. Some studies have indicated that alendronate sodium can strongly bind to calcium ions on the surface of bone hydroxyapatite through non-covalent interactions between the negatively charged bisphosphonate groups and the positively charged calcium ions on the hydroxyapatite surface [20]. Based on this theory, we combined hyaluronic acid methacrylate chains with alendronate sodium and utilized photo-crosslinking to form a three-dimensional dynamic molecular network hydrogel.

Incorporating bioactive glass into hydrogels has been shown to significantly improve their mechanical properties, addressing the issue of insufficient strength. Mesoporous bioactive glass (MBG) is an inorganic material with an ordered mesoporous structure and high specific surface area, offering robust drug-loading capabilities and broad application prospects [21,22]. MBG synthesized via a templating agent, composed of SiO_2-P_2O_5-CaO, facilitates the formation of a hydroxyapatite layer on its surface. On one hand, the primary degradation products of MBG, Ca^{2+} and PO_4^{3-} ions, provide raw materials for apatite deposition in the biomineralization process *in vivo*. The calcium ions released from the surface of MBG interact with ALN, also facilitating the aggregation of hydrophilic polymer chains to form a three-dimensional physical network. On the other hand, the *Si*-O functional groups in MBG act as active sites, offering greater potential for drug binding. Hydroxyapatite, an inorganic component with excellent biocompatibility, high bioactivity, and superior osteoconductivity, can be introduced into injectable hydrogels to better mimic the composition of bone tissue and significantly improve the osseointegration of implants with bone tissue.

Inspired by this, we designed MBG microspheres loaded with dopamine-grafted osteogenic peptides to enhance the osteogenic performance of the material. We then fully integrated these osteogenic peptide-loaded MBGs with photocrosslinked hydrogels to create a dual-carrier drug delivery system for treating osteoporosis. The nanocomposite material we developed, combining mesoporous bioactive glass with hyaluronic acid, effectively mimics the organic-inorganic composition of bone tissue, promotes osteoblast differentiation, inhibits osteoclastogenesis, and effectively aids in the repair of osteoporotic bone defects (Scheme 1).

2. Material and method

2.1. Synthesis of HAMA-ALN

Hyaluronic acid (HA, 40–100 kDa) was purchased from Macklin. Methacrylate hyaluronic acid (HAMA) was synthesized according to the method reported in the literature. Briefly, HA was dissolved in deionized water (pH 8.0) and reacted with 3 molar equivalents of methylacryloxyethyl (Aladdin, China). The reaction proceeded for 2 h, followed by continuous stirring at low temperature for 24 h. Upon completion, the reaction mixture was subjected to dialysis using a 3.5 kDa MWCO SNAKESKIN dialysis membrane (Thermo Feil) against deionized water, with the dialysate replaced every 6 h for a total of four cycles. The purified HAMA was then obtained by freeze-drying for 72 h.

To synthesize HAMA-ALN, 1 g of HAMA was dissolved in 70 mL of PBS (Solarbio) along with 0.5 g of EDC (Macklin) and 0.3 g of NHS (Sigma). The mixture was stirred at room temperature for 3 h to activate the carboxyl groups on the HA side chains, yielding HAMA-NHS. Separately, 800 mg of ALN (YuanYe) was dissolved in 30 mL of PBS by ultrasonic agitation and heating in a 40 °C water bath to ensure complete dissolution. The HAMA-NHS solution was then mixed with the ALN solution and stirred thoroughly for 3 days. After the reaction, the mixture was dialyzed against deionized water for purification. The final product, a white spongy material designated as HAMA-ALN, was obtained via freeze-drying. The degree of modification of HAMA-ALN was determined using 1H NMR analysis (Bruker, 400 MHz) in deuterium oxide (Sigma-Aldrich).

2.2. Synthesis of MBG@D5

MBG was synthesized using the surfactant template method, with hexadecyltrimethylammonium bromide (CTAB, Sigma) as the template. Briefly, 7.092 g of Tris-HCl powder was dissolved in 250 mL of deionized water at 60 °C, followed by the addition of 1.5 g of CTAB. After the solution became clear, 10.8 mL of tetraethyl orthosilicate (TEOS), 0.9 mL of triethyl phosphate (TEP), and 2.45 g of calcium nitrate tetrahydrate ($Ca(NO_3)_2{\cdot}4H_2O$) were sequentially added. The mixture was stirred gently at 200 rpm for 30 min and then vigorously at 800 rpm for 16 h until the solution turned milky white. The resulting precipitate was collected and washed three times alternately with anhydrous ethanol and deionized water, followed by centrifugation at 5000 rpm for 30 min. The solid was dried in an oven at 60 °C for 24 h, ground into a fine powder, and calcined in air at 650 °C for 3 h to obtain MBG nanoparticles. The peptide D5 was synthesized by Shanghai Qiangyao Biotechnology Co., Ltd., using the Fmoc solid-phase peptide synthesis method. Under sterile conditions, 5 mg of lyophilized D5 was dissolved in 5 mL of PBS (pH 7.4), and 10 mg of MBG nanoparticles was added. The mixture was stirred at 500 rpm for 2 h, followed by centrifugation at 2000 rpm for 5 min to remove the supernatant. The unattached free peptides were removed by washing with deionized water. The final MBG@D5 nanoparticles were obtained by freeze-drying overnight.

2.3. Preparation of composite hydrogels

To prepare the MBG@D5-Gel composite hydrogel, 1 % (wt) MBG particles were added to a 2 % (w/v) HAMA solution, which is dissolved in a 0.25 % (w/v) photoinitiator LAP standard solution. The mixture was stirred using a magnetic stirrer for 1 h. The pre-stirred hydrogel solution was then subjected to ultrasonic treatment to further disperse the MBG

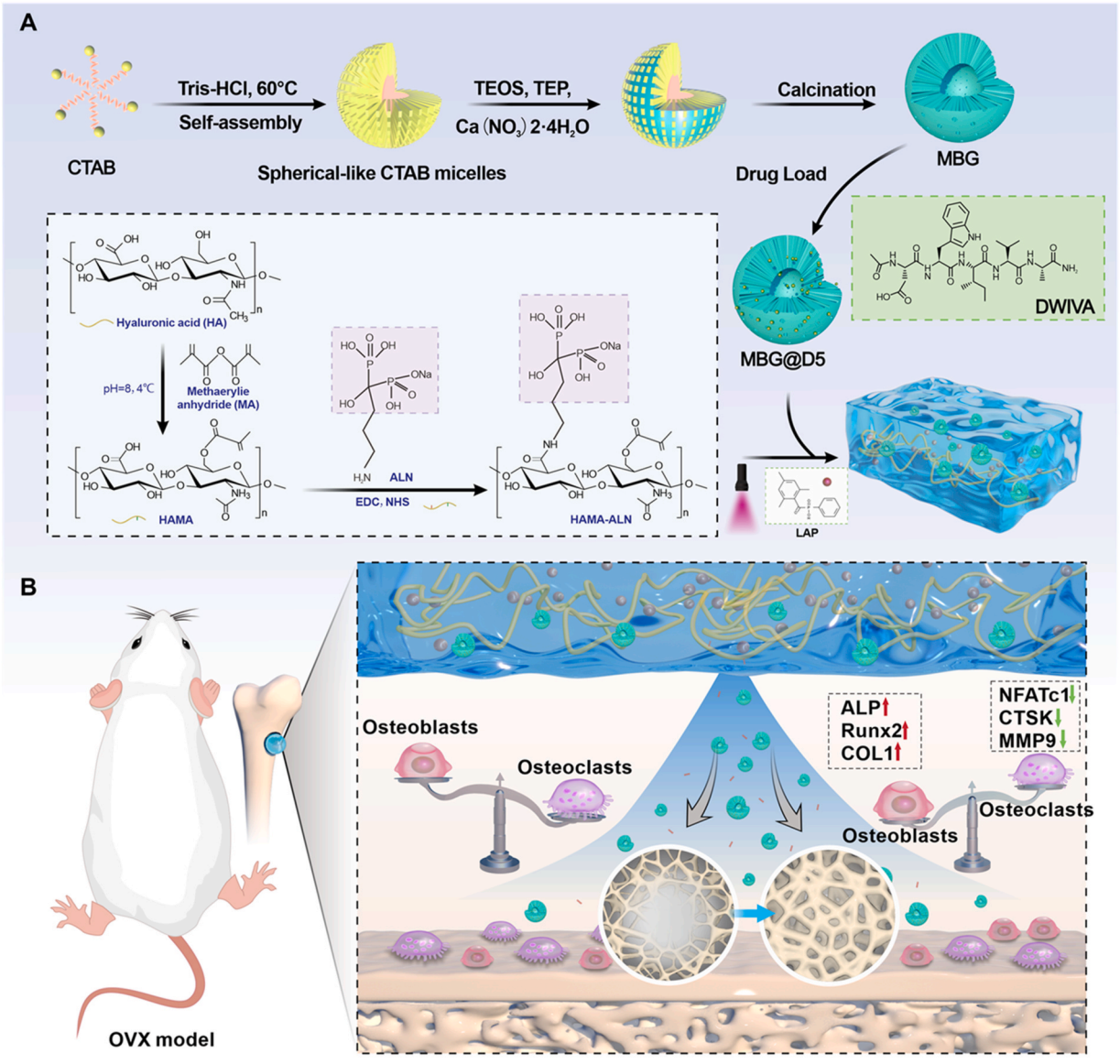

Scheme 1. The synthesis and preparation of the composite hydrogel enables the repair and regeneration of osteoporotic bone defects by promoting osteogenic differentiation and inhibiting osteoclastic differentiation.

particles evenly. Finally, the mixture was exposed to light at a wavelength of 405 nm for 1 min to induce photocrosslinking, resulting in the formation of the composite hydrogel, named MBG@D5-Gel.

2.4. Characteristics of materials

High-resolution transmission electron microscopy (TEM) images and elemental mapping were acquired using a JEM-2100F microscope. The particle size distribution and average particle size of the MBG particles were analyzed using Image J software.

The rheological properties of the gel were characterized using a stress-controlled rheometer (TA Instruments, UK). Cylindrical gel sample with a diameter of 3 cm and a thickness of 0.3 cm were placed on a parallel plate (40 mm Peltier plate steel). The measurements was conducted at a constant temperature of 37 °C. To determine the initial storage modulus (G′) and loss modulus (G″), the gel was subjected to a strain of 1 % for 3 min. Subsequently, the frequency-dependent behavior of the gel was evaluated by measuring changes in G′ and G″ across a shear frequency range of 0.1 rad/s to 50 rad/s. The critical strain and linear viscoelastic region (LVR) were determined by applying a constant shear frequency of 10 rad/s while varying the dynamic strain from 0.1 % to 300 %, and monitoring changes in G′ and G". The self-healing properties of the hydrogel were assessed using failure-recovery tests. These tests involved applying alternating cycles of high strain (beyond the LVR) and low strain (within the LVR), with the corresponding changes in G′ and G″ recorded. All measurements were performed in duplicate to ensure reproducibility.

The surface morphology of dried MBG-Gel was examined using a scanning electron microscope (SEM, Hitachi, Japan). Samples were mounted on conductive adhesive and secured to the SEM sample stage. The surfaces were gold-coated under vacuum conditions to enhance conductivity before imaging. Surface morphology was then observed, and images were captured using SEM.

To measure the swelling rate of the mixed hydrogel samples, 300 μL of the mixed hydrogel solution was added to cylindrical plastic molds. Each group of hydrogel solutions was then exposed to ultraviolet light at a wavelength of 405 nm for 60 s to initiate photopolymerization. After the photopolymerization process, the hydrogel samples, with or without MBG, were placed in Eppendorf tubes containing 2 mL of PBS and incubated for 24 h to reach equilibrium. After 24 h, the swollen

hydrogels were weighed, and excess water was gently blotted off with a paper towel. Four replicate samples were used for each hydrogel group. The swelling rate of the hydrogel was calculated using the following formula: Swelling ratio = [(Ww − W0)/W0], where Ww is the wet weight of the hydrogel sample, and W0 is the dry weight of the hydrogel sample.

2.5. In vitro drug release experiment

The *in vitro* release of ALN and D5 from the hydrogel system was investigated at 37 °C in an incubator. A total of 1 mL of drug-loaded hydrogel solution was added to 15 mL centrifuge tubes. The total drug loading was calculated based on the grafting rate of ALN and D5, respectively. The hydrogel system was then covered with 2 mL of pre-heated PBS (pH 7.4) and gently shaken at 100 rpm at 37 °C.

At predetermined time points, half of the release medium was collected and replaced with an equal volume of fresh preheated PBS. All collected release media were stored at −20 °C for subsequent analysis. The drug release profiles were determined using high-performance liquid chromatography (HPLC). Standard curves were established by measuring the HPLC responses of solutions with known concentrations.

2.6. Biocompatibility testing

Cell viability in co-culture with hydrogels was assessed using a Live/Dead Cell Viability Assay Kit (Solarbio, China). Hydrogel-loaded cells were incubated with 2 μM calcein AM and 8 μM propidium iodide (PI) in the kit's buffer solution at 37 °C for 1 h, following the manufacturer's protocol. After incubation, the samples were washed three times with buffer, and fluorescence images were captured using an inverted fluorescence microscope. To further evaluate cell viability, a CCK-8 assay was performed. Cells were co-cultured with hydrogels in a 96-well plate as per the kit's instructions, and cell viability was assessed after a specific period of incubation in proliferation medium.

The hemocompatibility of the hydrogels was evaluated using a red blood cell (RBC) hemolysis assay. Fresh blood samples were collected from SD rats via cardiac puncture under anesthesia. RBCs were separated from plasma by centrifugation and washed three times with sterile saline. The RBCs were then diluted to a 2 % (v/v) solution in sterile saline and mixed with each hydrogel group. The mixtures were left to stand at room temperature for 1 h. RBCs diluted in deionized water and saline were used as positive and negative controls, respectively. Following 2 h of incubation, the samples were centrifuged at 3000 rpm for 5 min at room temperature. Hemolysis photographs were captured, and the absorbance of the supernatant was measured at 570 nm using a UV spectrophotometer.

2.7. Cell culture and osteogenic differentiation

Bone marrow-derived mesenchymal stem cells (BMSCs) used in this study were extracted from SD rats following established methods. Briefly, the femoral marrow cavity was flushed under sterile conditions to collect the marrow tissue. The samples were lysed, washed, and centrifuged at 1000 rpm for 5 min. The supernatant was discarded, and the resulting cell pellet was resuspended in 8 mL of complete medium consisting of α-MEM (low glucose; Gibco, USA) supplemented with 10 % fetal bovine serum (FBS; Gibco, USA) and 1 % penicillin/streptomycin (Gibco, USA). The cells were seeded into culture dishes and incubated at 37 °C in a humidified atmosphere containing 5 % CO_2. The medium was changed every other day until the cells reached 80 % confluence. Cells from passage 3 to 5 were used for subsequent experiments.

The osteogenic differentiation induction medium was prepared using α-MEM supplemented with 10 % FBS, 10 mM β-glycerophosphate, 50 μM ascorbic acid, and 100 nM dexamethasone (Solarbio).

2.8. Alkaline phosphatase staining and quantification

BMSCs were seeded at a density of 2×10^4 cells per well in 24-well plates. After cell adhesion, the cells were co-cultured with various materials and induced for osteogenic differentiation. On day 7 of induction, the cells were fixed with 4 % paraformaldehyde, permeabilized with 0.1 % Triton X-100, and stained using a BCIP/NBT alkaline phosphatase staining kit (Solarbio, China). ALP activity was quantified using a commercial ALP activity quantification kit (Solarbio, China), following the manufacturer's protocol.

2.9. Alizarin red staining

To assess calcium mineralization, BMSCs were cultured with various hydrogels for 21 days. The cells were fixed with 4 % paraformaldehyde, washed with PBS, and stained with 2 % alizarin red S solution (Solarbio, China) at room temperature for 30 min. Excess dye was removed by washing with deionized water, and the stained samples were observed under an optical microscope. For quantification of calcium deposition, 10 % cetylpyridinium chloride was added to dissolve the mineralized nodules. The optical density (OD) was measured at 562 nm using a microplate reader.

2.10. Cell culture and osteoclast differentiation

Primary bone marrow macrophages (BMMs) were isolated from rat bone marrow to evaluate the biological effects of various nanomaterials (40 μg/mL) on osteoclastogenesis. The BMMs were cultured in α-MEM supplemented with 1 % penicillin/streptomycin, 15 % bovine serum, and 25 ng/mL recombinant mouse M-CSF (R&D Systems, Minneapolis, MN, USA) for 24 h. Subsequently, the cells were incubated for an additional 3–5 days to allow full fusion. The fused BMMs were seeded into 96-well plates at a density of 1×10^5 cells/well and treated with specified concentrations of hydrogel materials in the presence of recombinant mouse RANKL (50 ng/mL) and M-CSF (25 ng/mL) from R&D Systems.

2.11. In vitro osteoclast formation assay

After 5 days of co-culture with different hydrogel materials, mature osteoclasts were fixed in PBS containing 4 % paraformaldehyde (Solarbio) for 20 min for TRAP staining. The cells were then stained using an acid phosphatase assay kit (TRAP, Sigma-Aldrich) according to the manufacturer's protocol to assess TRAP activity. Stained cells were imaged using an optical microscope (Leica Microsystems). The area and number of TRAP-positive cells, indicative of differentiated multinucleated osteoclasts, were quantified in randomly selected fields of view.

To evaluate the bone resorption function of osteoclasts, bovine bone slices were utilized. The cells were incubated on the bone slices, followed by osteoclast induction in a 48-well plate. After incubation, Trizol was used to remove the cells from the surface, allowing the observation of resorption pit formation using SEM.

2.12. Determination of osteogenic and osteoclastic gene and protein expression

Real-time polymerase chain reaction (RT-PCR) was employed to detect the mRNA expression of markers related to bone formation, including alkaline phosphatase (ALP), Runx2, osteocalcin (OCN), SP7, and osteopontin (OPN), as well as markers associated with osteoclast formation, such as TRAcP, MMP9, and Nfatc1. Total RNA (40 μg/mL) was extracted from cells co-cultured with hydrogels using TRIzol reagent (Invitrogen, Thermo Fisher Scientific) according to the manufacturer's instructions. The RNA concentration was measured with a NanoDrop spectrophotometer (ND-1000, Thermo Fisher Scientific), and cDNA templates were synthesized from the extracted RNA using the All-

In-One RT MasterMix kit (Novizan Biotechnology Co., LTD.). Quantitative RT-PCR was then conducted using the ChamQ SYBR qPCR Master Mix kit (Novizan Biotechnology Co., LTD.). Forward and reverse primer sequences were synthesized by Sangon Biotech Ltd., Shanghai, China, as listed in Table S1. Gene expression levels were normalized to glucose-6-phosphate dehydrogenase (GAPDH), which served as an internal reference.

Western blot analysis was conducted to examine the expression of osteoblast proteins in BMSCs treated with an osteogenic differentiation induction medium. Total proteins were extracted from the BMSCs and separated using a 10 % SDS-PAGE gel. The separated proteins were then transferred onto a PVDF membrane (Millipore, USA) and blocked with 5 % skim milk in TBST. The membrane was incubated overnight at 4 °C with the primary antibodies: anti-COL1 (1:2000; Abcam), anti-RUNX2 (1:2000; Abcam), anti-ALP (1:2000; Abcam), and anti-β-actin (1:5000; Abcam). After three washes with TBST, the membrane was incubated with anti-rabbit IgG at room temperature for 1 h. This was followed by a final incubation with the secondary antibody at room temperature for 2 h. The protein bands were then visualized using enhanced chemiluminescence and analyzed with Bio-Rad Image Lab software 5.2 (Bio-Rad Laboratories, Hercules, CA, USA).

2.13. Establishment of an osteoporosis and bone defect animal model

Female SD rats (200 ± 20 g) were obtained from the Laboratory Animal Center of Soochow University (Suzhou, China). Prior to surgery, all rats were housed in a specific pathogen-free (SPF) environment for one week with free access to food and water. The animal experiment was approved by the Ethics Committee of Soochow University and was conducted humanely throughout the study (SUDA20240415A04).

A bilateral oophorectomy (OVX) or sham surgery was performed following established protocols. Under sterile conditions, the rats' backs were disinfected with iodine solution and medical alcohol, and they were positioned prone. The skin on the back was incised, both ovaries were removed, and the fallopian tubes were ligated. In the sham group, the fat surrounding the ovaries was removed similarly. One month post-operation, the osteoporosis model was validated using micro-CT and histological examination.

After confirming the successful establishment of the osteoporosis model, the rats were randomly divided into four groups. A femoral defect model was then created, and the material was implanted. Specifically, an oblique incision (~1 cm) was made on the medial side of the distal femur joint. The fascia and muscle were bluntly separated to expose the bone. A non-penetrating defect, 4 mm deep, was created by placing the surgical implant (2 mm in diameter) 1 mm below the cartilage growth plate, perpendicular to the bone surface. Then the HAMA, MBG, and LAP pre-mixture (MBG-Gel or MBG@D5-Gel) was injected into the defect site using a 5 mL syringe. The mixture was then cured by applying local 405 nm ultraviolet light irradiation for 60 s. Subsequently, each layer of subcutaneous tissue was sutured. The defect was filled with composite gel. Three days post-surgery, penicillin (800,000 units) was administered according to standard protocol.

2.14. Micro computed tomography (Micro-CT) analysis

At predetermined time points after surgery (4 and 12 weeks), the animals were euthanized, and their femurs were harvested. The femurs were then fixed in 4 % formalin solution. Morphological assessments (n = 5) were performed on the femurs from each group using a high-resolution micro-computed tomography scanner (μCT 80, Scanco Medical, Buttikon, Switzerland).

The scanning parameters were as follows: resolution of 18 μm, voltage of 50 kV, current of 500 μA, and an exposure time of 100 ms per image, with 0.9° rotation per 8 images. The femoral condyle defect was selected as the region of interest, and the images were reconstructed using Micro-CT image analysis software to analyze and quantify the healing of the defect area. The following morphological parameters were recorded: bone volume to total volume ratio (BV/TV), bone mineral density (BMD), trabecular thickness (Tb.Th), trabecular spacing (Tb.Sp), and pore number.

2.15. Histological examination histological examination

To further evaluate the osteogenic and anti-inflammatory effects of the hydrogel, the samples were stained with hematoxylin-eosin (H&E), Masson's capillaries, immunohistochemical (IHC) staining, and immunofluorescence staining. At predetermined time points (3, 6, and 9 weeks), the animals were put to death and samples were taken from their femurs. The sample was then fixed with 4 % formalin and decalcified with 12.5 % ethylenediamine tetraacetic acid (EDTA). H&E staining was performed on the samples according to the standard procedure to observe the changes of bone histomorphology. TRAP dyeing and Masson dyeing were performed simultaneously. Histological sections were observed under a bright microscope (Zeiss, Germany) and the number of TRAP-positive multinucleated osteoclasts in selected areas was quantified.

Based on previous studies, histopathological analysis of major organs in rats and biochemical assessment of blood samples were performed to determine the *in vivo* biosafety of the hydrogel. Specifically, prior to sacrificing the rats, cardiac perfusion fixed tissue, which was cut from the heart, lungs, spleen, liver, and kidneys of each group (n = 4) of rats, and stained with an H&E staining kit to observe the tissue structure.

2.16. Statistical analysis

Statistical analysis was performed using GraphPad Prism 9.0 software (GraphPad Software, USA). Data are presented as mean ± standard deviation (SD). Comparisons between multiple groups were conducted using one-way analysis of variance (ANOVA) followed by Tukey's post-hoc test. P-values <0.05 were considered statistically significant.

3. Results

3.1. Fabrication and characterization of MBG@D5-Gel

The preparation of MBG and the process of modifying it with DWIVA polypeptide grafted by DOPA on both the surface and within the mesopores are illustrated in Fig. 1A. Transmission electron microscopy (TEM) was employed to verify the morphology of MBG. As shown in Fig. 1B, MBG exhibits a uniform, near-spherical shape with clearly visible pores evenly distributed across each particle's surface, forming a mesoporous structure radiating from the center to the exterior. Dynamic light scattering (DLS) was used to measure the average particle size of MBG, which was approximately 257.5 nm, as depicted in Fig. S1. Elemental analysis mapping (Fig. 1C) confirmed that calcium, silicon, and phosphorus were uniformly distributed within MBG, further validating its successful synthesis.

ALN is a widely used clinical anti-bone resorptive drug, commonly employed to alleviate osteoporosis. Fig. 1D provides a schematic of the HAMA-ALN preparation process. To create HAMA-ALN, we used the EDC/NHS method to covalently attach ALN to HAMA through amide bonds formed by an amine group exchange reaction (Fig. 1D). Additionally, ^{1}H NMR analysis was performed to investigate the methacrylation of the biopolymer HAMA and the binding of ALN to HAMA macromolecules through chemical bonds. As shown in Fig. 1E, the ^{1}H NMR spectrum of HAMA exhibited methacrylate peaks at 5.5 and 6.2 ppm, in contrast to the ^{1}H NMR spectrum of HA. The peak at 1.9 ppm corresponds to the methyl proton of the grafted methacryloyl group (CH=CH(CH)), which is absent in the unmodified HA spectrum. Further comparative analysis of the ^{1}H NMR spectra revealed that, in addition to the original methyl proton peak (1.9 ppm), a new set of peaks appeared in the synthesized HAMA-ALN spectrum, corresponding to methylene

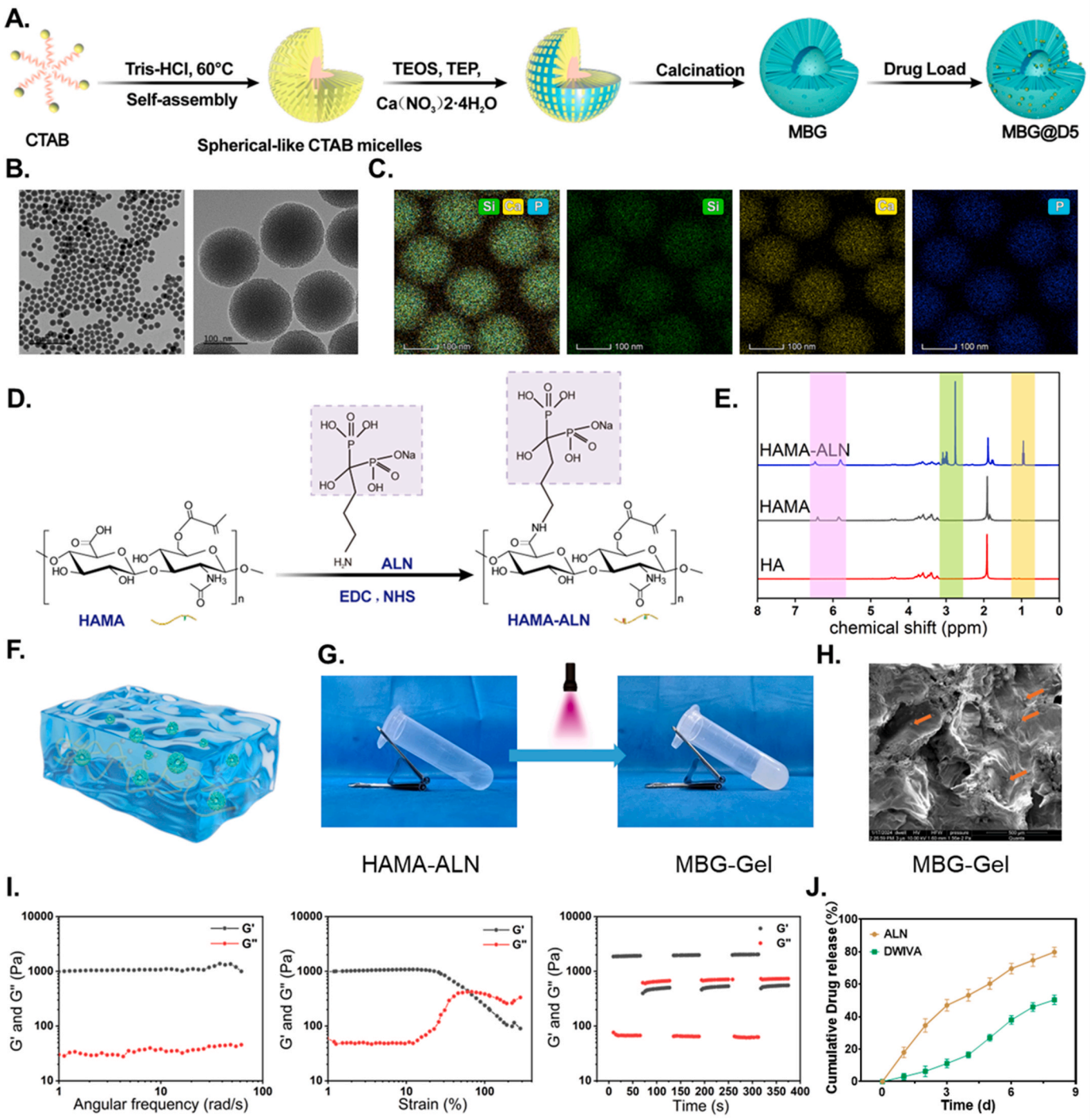

Fig. 1. Fabrication and characterization of HAMA-ALN and MBG-Gel. (A) Schematic diagram of MBG synthesis. (B) TEM image of MBG. (C) Mapping analysis. (D) Schematic diagram of HAMA-ALN synthesis. (E) ^{1}H NMR spectra (600 MHz) of HA, HAMA and HAMA-ALN in D_2O. (F) Schematic diagram of MBG@D5-Gel. (G) Solution containing HAMA-ALN and MBG@D5 underwent gelation at LAP and 405 nm wavelength illumination. (H) SEM images of MBG-Gel. (I) Spectrum of elastic (G′) and viscous (G″) modulus of MBG-Gel with varying strain, frequency, and time applied. (J) Drug release of ALN and D5 peptide.

protons at 2.9 ppm, 0.9 ppm, and 1.8 ppm. This indicates successful binding of ALN to HAMA.

Based on the interaction between LAP and Methacrylic acid group, we used 405 nm light to cross-link HAMA-ALN with MBG (Fig. 1F). After MBG added and 405 nm light exposed, the solution transformed from a liquid to a gel state, with its color changing from colorless and transparent to white, which is attributed to the inherent color of MBG (Fig. 1G). Scanning electron microscopy revealed that the pore size within MBG-Gel was uniformly distributed, with MBG particles evenly dispersed on the surface. Rheological tests showed that the elastic modulus (G′) of MBG-Gel, which contains MBG particles, was higher than its viscous modulus (G″), with crossover points indicating the structural integrity of the hydrogel. The effects of ALN, D5, and MBG on the swelling properties of HAMA hydrogels were investigated by measuring the equilibrium swelling rates of hydrogels with different components in PBS. As shown in Fig. S2, none of these components significantly affected the equilibrium swelling rate of the HAMA hydrogel.

Subsequently, we synthesized a hydrogel, MBG@D5-Gel, containing both ALN and D5 peptides as dual-function molecules. We investigated its drug release profile in the gel state. The results demonstrated that ALN had a peak release rate within the first three days, while the release of the D5 peptide was slower, reaching only 20 % by day 9. This difference in release rates is likely due to ALN being released in conjunction with the degradation of the hydrogel, whereas the D5 peptide is bound to MBG via DOPA. These findings indicate that we have successfully synthesized an organic-inorganic hybrid hydrogel capable of carrying and releasing bifunctional drugs.

3.2. Biocompatibility of MBG@D5-Gel

Biocompatibility is essential for materials used in the biomedical field. To assess the cytotoxicity of composite hydrogels *in vitro*, BMSCs and BMMs were employed in subsequent experiments. BMSCs were co-cultured with the hydrogels to evaluate cell viability. Live/dead staining revealed that the majority of cells were stained green (indicating live cells), with only a few stained red (indicating dead cells) (Fig. 2A), demonstrating high cell viability. Additionally, the OD value from the CCK-8 assay increased over 1, 3, and 5 days of culture, suggesting that BMSCs not only thrived within the hydrogel but also proliferated effectively (Fig. 2B). Similarly, MBG@D5-Gel exhibited good biocompatibility with BMM cells (Fig. 2C and D). As illustrated in Fig. 2E, the MBG@D5-Gel exhibits no discernible hemolytic activity, with the hemolysis rate remaining below 5 % after 2 h of incubation. This suggests that the material is well-compatible with blood. Collectively, these results indicate that the MBG@D5-Gel hydrogel possesses excellent biocompatibility *in vitro*.

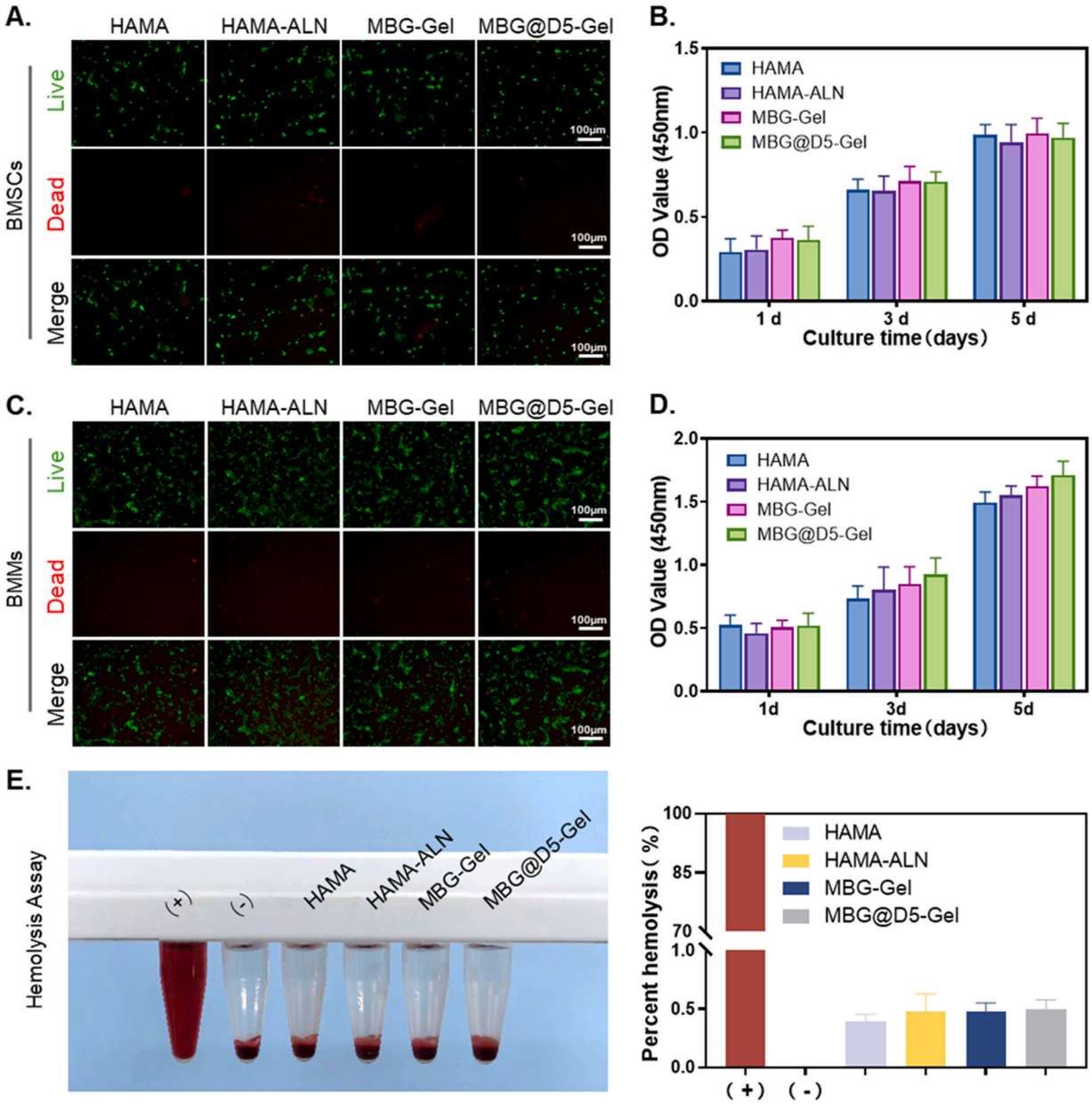

Fig. 2. *In vitro* biocompatibility evaluations of HAMA, HAMA-ALN, MBG-Gel and MBG@D5-Gel. (A) Live (green) and dead (red) cells of BMSCs after cultured with the extract. (B) Cell viability of BMSCs after cultured with the extract, (n = 5). (C) Live (green) and dead (red) cells of BMMs after cultured with the extract. (D) Cell viability of BMMs after cultured with the extract, (n = 5). (E) Hemolysis Rate of red blood cells in different treated with HAMA, HAMA-ALN, MBG-Gel and MBG@D5-Gel. (For interpretation of the references to color in this figure legend, the reader is referred to the Web version of this article.)

3.3. MBG@D5-gel promoted osteogenic differentiation of BMSCs

To further validate the bone-inducing activity of the hydrogels, ALP and ARS staining were conducted to assess early and late osteogenic differentiation of BMSCs on different hydrogel formulations. ALP staining results (Fig. 3A) demonstrated that BMSCs in the MBG@D5-Gel group exhibited more extensive ALP-positive areas and higher staining intensity after 7 days compared to the MBG-Gel group, which lacked osteogenic peptides. Analysis of ALP activity in cell lysates confirmed that the hydrogel containing osteogenic peptides induced stronger early bone differentiation than the MBG-only hydrogel (Fig. 3B). After 21 days, calcium nodule formation was significantly enhanced in both the MBG-Gel and MBG@D5-Gel groups, with quantitative analysis of dissolved calcium nodules aligning with the observed results (Fig. 3C and D). Additionally, qPCR was employed to examine changes in the expression levels of early and late osteogenic genes. The expressions of early osteogenic markers Runx2, Alp, and Sp7, as well as late osteogenic markers OPN and OCN, were significantly upregulated in the MBG@D5-Gel group, correlating with the release of the polypeptides (Fig. 3E).

The expression of Runx2 in BMSCs co-cultured with the hydrogel was directly assessed using immunofluorescence staining, as shown in Fig. 3F. On the 4th day of co-culture with the MBG@D5-Gel, BMSCs

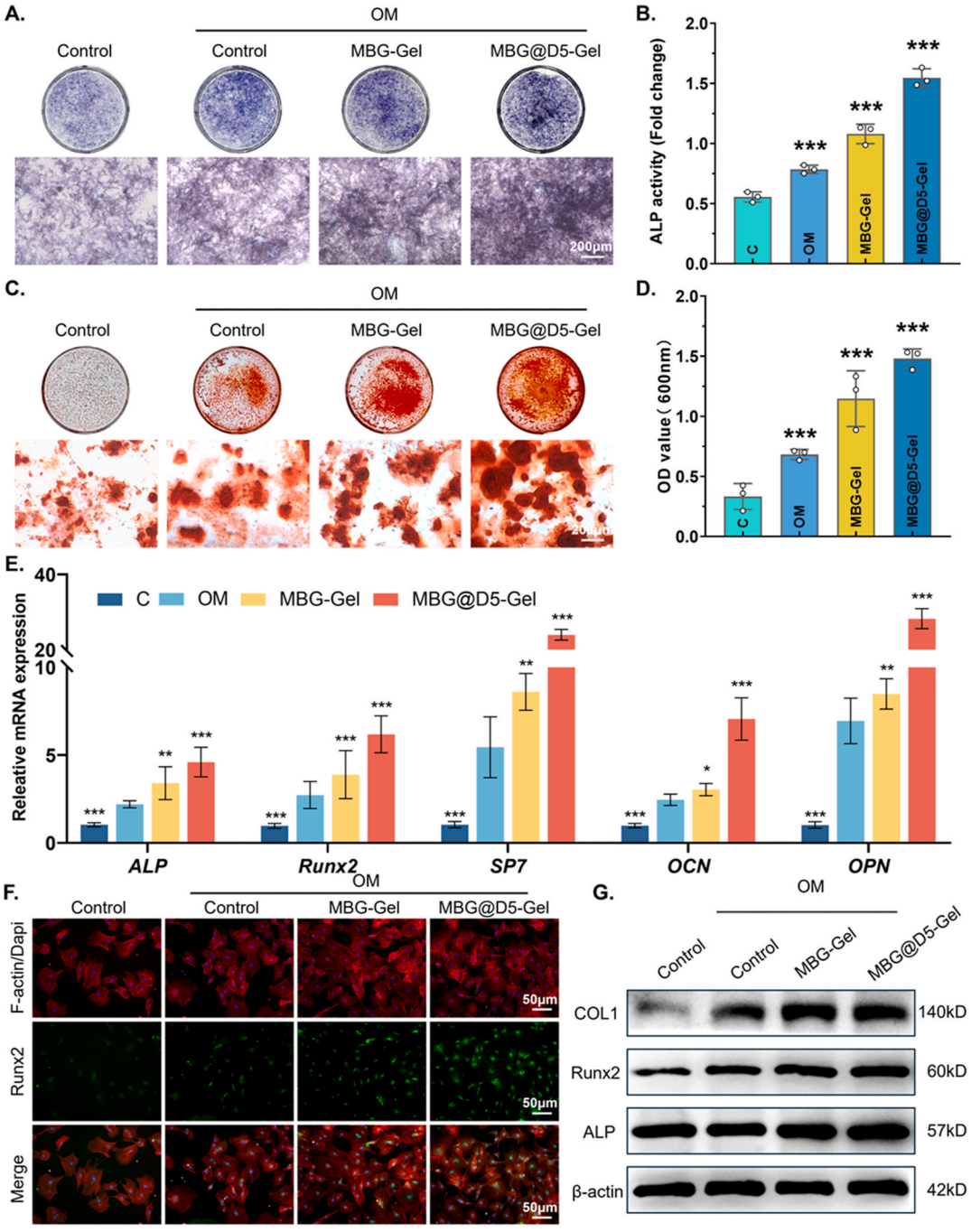

Fig. 3. *In vitro* osteogenic properties of the dual functional hydrogel. (A) ALP staining. (B) Quantitative evaluation of ALP activity. (C) Alizarin red S staining. (D) Semiquantitative evaluation of ECM mineralization. (E) Gene levels of ALP, Runx2, SP7, OCN, and OPN. (F) Immunofluorescence staining of Runx2 (green). (G) Western blotting of COL1, Runx2, ALP and β-actin in BMSCs after different treatments. (*** denotes $p < 0.001$ compared to the control group). (For interpretation of the references to color in this figure legend, the reader is referred to the Web version of this article.)

exhibited the highest RUNX2 fluorescence intensity. Western blot results (Fig. 3G) further confirmed that osteogenic induction in BMSCs was significantly enhanced in both the MBG-Gel and MBG@D5-Gel groups compared to the control group and the osteogenic induction medium group, with the latter showing a stronger regulatory effect than the former. This highlights the enhanced osteogenic differentiation mediated by D5.

These results indicate that the MBG@D5-Gel hydrogel, incorporating the D5 polypeptide, demonstrates excellent osteogenic induction capabilities by up-regulating the expression of osteogenic proteins and genes *in vitro*. This provides valuable experimental evidence for promoting bone defect regeneration *in vivo*.

3.4. MBG@D5-gel decreased the osteoclastogenesis of BMMs

BMMs were co-cultured with the hydrogel in the presence of M-CSF (macrophage colony-stimulating factor) and RANKL to investigate the effect of ALN release on osteoclast formation. As shown in Fig. 4A, the number of osteoclasts produced in the RANKL group was significantly higher compared to the Control group. When the Control group was replaced with co-cultures using MBG-Gel and MBG@D5-Gel incorporating ALN, a significant reduction in osteoclast induction by RANKL was observed, along with fewer TRAP-positive cells. Additionally, the bone resorption function of osteoclasts was inhibited, as evidenced by a smaller bone plate resorption area. This was confirmed by the quantitative analysis of TRAP-positive osteoclast regions and bone resorption areas (Fig. 4B and C). Ghost pen cyclic peptide staining, which visualizes the F-actin ring—a feature of functional osteoclasts—showed a distinct ring structure at the cell periphery in the RANKL group, with multinucleated cells. In contrast, the MBG-Gel and MBG@D5-Gel groups exhibited less osteoclast formation and smaller F-actin ring areas (Fig. 4D–F).

Bone resorption differentiation is associated with RANKL-mediated upregulation of specific genes, including TRAP, matrix metalloproteinase-9 (MMP-9), and NFATc1. qRT-PCR analysis revealed that RANKL stimulation significantly increased the expression of these genes in BMMs. The MBG-Gel and MBG@D5-Gel groups showed statistically significant differences in the mRNA expression of TRAP, MMP-9, and NFATc1, with results indicating RANKL > Control > MBG-Gel ≈ MBG@D5-Gel. Western blot analysis of cathepsin K, MMP-9, and NFATc1 also supported these findings, showing similar trends in protein expression levels (Fig. 4G).

In summary, composite hydrogels crosslinked with 405 nm light can effectively inhibit osteoclast differentiation and bone resorption *in vitro*.

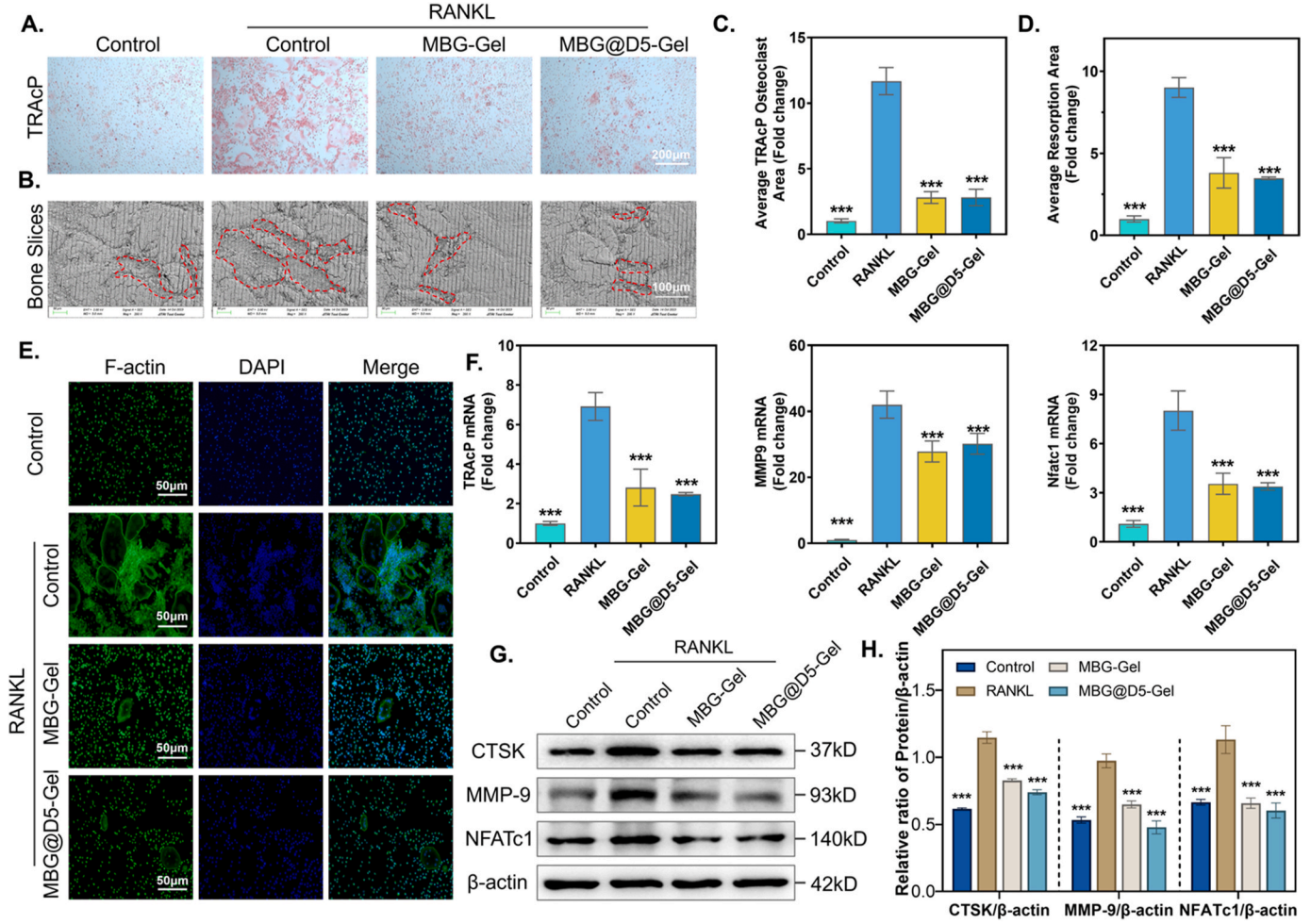

Fig. 4. *In vitro* osteoclastic properties of the dual functional hydrogel. (A) TRAP staining. (B) Bone resorption assays. (The red dashed square encloses bone resorption area) (C) Quantification of area of TRAP + multinuclear cells (D) Quantification of the area of resorption pits per bone slice. (E) Immunofluorescence staining using phalloidin (green) for F-Actin ring formation assays. (F) Gene levels of TRAcP, MMP9, and Nfatc1. (G) Western blotting of CTSK, MMP-9, and NFATc1 in BMMs after different treatments. (H) Quantitative analysis of Western blot results. (*** denotes $p < 0.001$ compared to the RANKL group). (For interpretation of the references to color in this figure legend, the reader is referred to the Web version of this article.)

3.5. MBG@D5-gel accelerated the bone healing of osteoporotic defect in rats

Based on the *in vitro* experiments confirming osteogenic-osteoclastic coupling, we further investigated the effects of the bifunctional hydrogel on bone defect regeneration and repair under osteoporotic conditions. To achieve this, we first established an osteoporosis rat model. In the first month following model establishment, rats were re-anesthetized, the femoral condyle was exposed, and the hydrogel for the corresponding group was implanted after manual drilling. This approach aimed to assess whether the MBG@D5-Gel could correct the osteogenic and osteoclastic imbalance in bone defects under osteoporosis and promote bone healing (Fig. 5A).

The effectiveness of the osteoporosis model was confirmed by three-dimensional reconstruction of the distal femur four weeks post-ovariectomy, evaluating bone parameters such as bone volume fraction (BV/TV), bone mineral density (BMD), trabecular thickness (Tb. Th), and trabecular number (Tb.N) (Fig. 5B). CT analysis of the distal condyle of the rat femur was performed at 4 and 12 weeks after hydrogel implantation. At both time points, newly generated bone tissue was observed in the damaged area, indicating progressive reconstruction (Fig. 5C). In contrast, the OVX group displayed significant loss of bone trabeculae, slow bone tissue growth, and limited bridging. In the MBG-Gel and MBG@D5-Gel groups, bone tissue grew centrically, defect

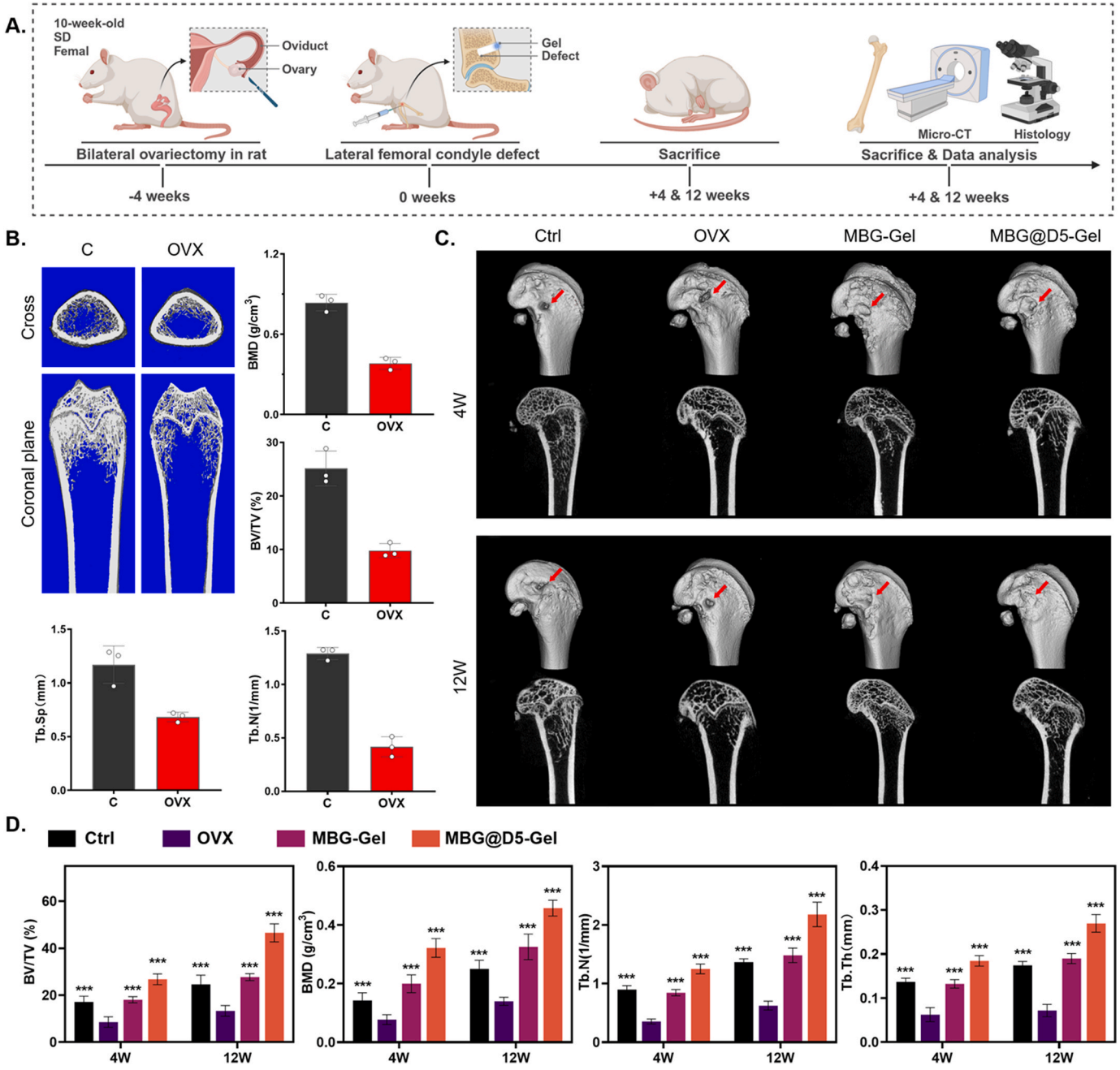

Fig. 5. In vivo evaluation of bone regeneration effect of dual functional hydrogel implanted in osteoporotic rat model with bone defect. (A) Schematic illustration showing the design of animal experiments. (B) Representative 3D reconstructed images of the OVX rat distal femurs and quantitative parameters of trabecular bone, BMD, bone mineral density; BV/TV, bone volume/tissue volume ratio; Tb. Sp, trabecular separation; Tb. N, trabecular number. (C) Representative 3D reconstructed images of bone defect of the 4 and 12 weeks. (Red arrow refers to the area of defect) (D) Quantitative parameters of trabecular bone in the defect area. (*** denotes $p < 0.001$ compared to the OVX group). (For interpretation of the references to color in this figure legend, the reader is referred to the Web version of this article.)

healing occurred, and trabecular bone loss around the defect was alleviated. Analysis of bone-related parameters at the defect site (Fig. 5D) revealed that the MBG@D5-Gel group exhibited the highest total bone tissue formation (BV/TV) and trabecular thickness (Tb.Th), followed by MBG-Gel. Notably, new bone tissue regeneration increased over time in all groups except the OVX group.

Histological analysis using H&E and Masson staining was conducted to understand the resistance mechanism to osteoporotic bone defects *in vivo*. H&E staining was employed to observe connective tissue, while Masson staining assessed bone maturity, with mature bone tissue appearing deep red. Bone tissue regeneration patterns within porous scaffolds were evaluated at weeks 4 (Fig. 6A) and 12 (Fig. 6B). At 4 weeks, bone formation in the Ctrl and OVX groups was limited, with the bone defect mainly filled with connective tissue and only a small amount of new bone at the defect edges. In the MBG-Gel and MBG@D5-Gel groups, sparse bone trabeculae extended into the defect area. The OVX group exhibited significant bone loss and limited trabecular regeneration, with the 12-week OVX group showing more trabecular bone distribution compared to the 4-week OVX group, though the structure remained disorganized and many cavities still appeared empty. By week 12, the MBG-Gel and MBG@D5-Gel groups displayed further filling of the defect area with newly regenerated, regular trabecular bone. Notably, the MBG@D5-Gel group showed accelerated defect healing, continuous bone-like tissue bridging at all time points, and the most pronounced new trabecular bone growth, consistent with the micro-CT findings.

The level of osteoclasts was assessed using TRAP staining. In the MBG-Gel and MBG@D5-Gel groups, TRAP staining revealed a significant reduction in both the number and percentage of osteoclasts on the bone surface, approaching normal levels (Fig. 6C). An increase in osteoclasts was observed in both cortical and cancellous bone regions.

To further confirm the biocompatibility of the MBG@D5-Gel implant, major organs such as the heart, liver, spleen, kidneys, and intestines were examined using H&E staining (Fig. 7). No significant pathological changes, such as necrosis or inflammation, were detected in any of the organ sections. These results indicate that MBG@D5-Gel exhibits good biocompatibility *in vivo*.

4. Discussion

Bone is a highly dynamic tissue, and its health relies on the precise balance between osteoblasts, which are responsible for bone formation, and osteoclasts, which mediate bone resorption. Disruption of this balance can lead to bone diseases like osteoporosis, characterized by excessive bone resorption and inadequate bone formation, resulting in reduced bone density and a compromised trabecular structure [23]. Consequently, bone healing in osteoporotic patients is impaired, making the treatment of osteoporotic bone defects more challenging than that of normal bone defects [24]. The high incidence of osteoporotic fractures underscores the urgent need to develop materials that can modulate the balance between osteogenesis and osteoclastogenesis to promote the regeneration of osteoporotic bone defects.

Bone regeneration is a continuous process wherein osteoclast-mediated bone resorption is gradually replaced by osteoblast-mediated

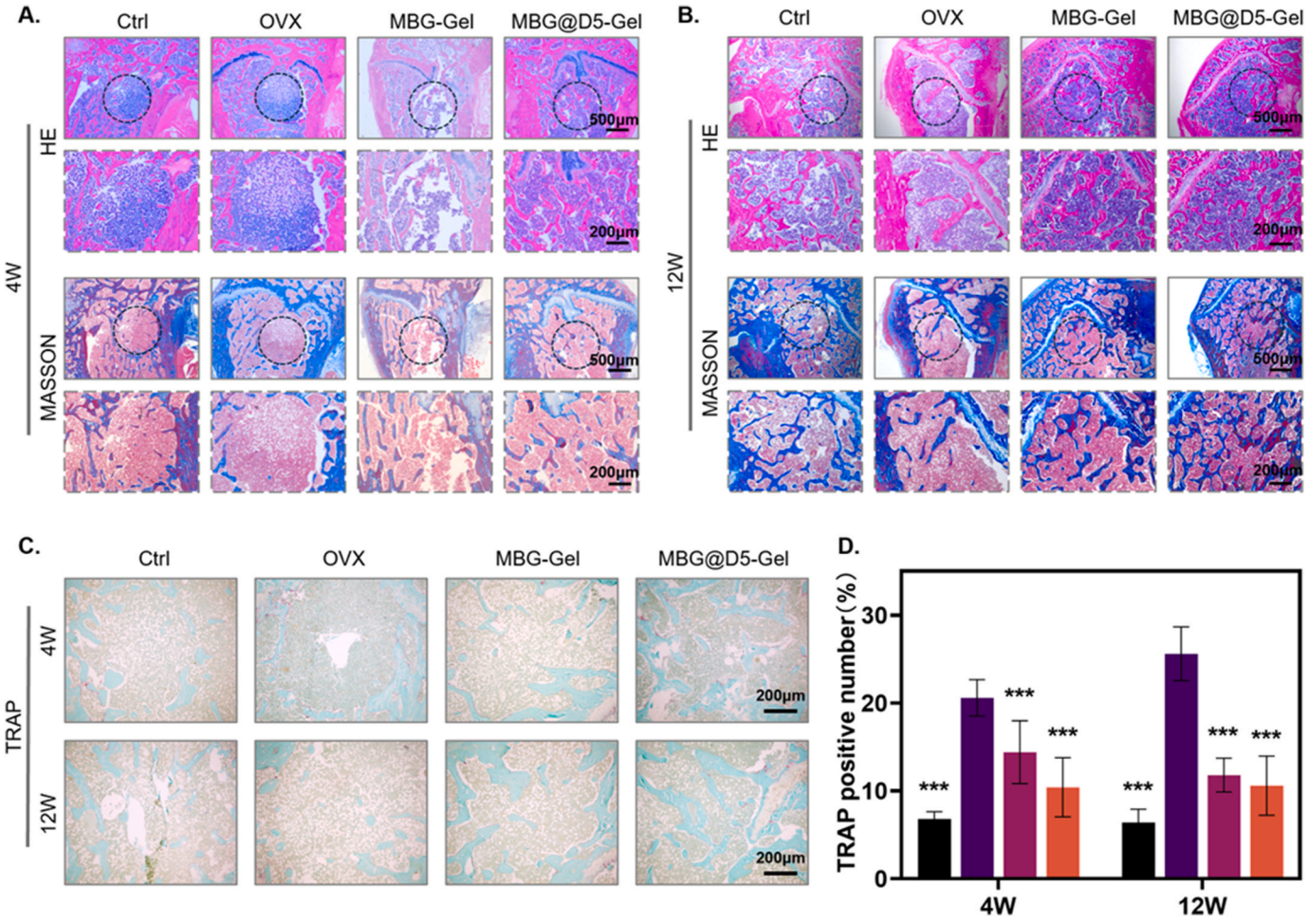

Fig. 6. Histological analysis in the bone defect area. (A) H&E staining and Masson staining of bone defect area of 4 weeks. (B) H&E staining and Masson staining of bone defect area of 12 weeks. (C) TRAP staining. (D) Quantitative analysis of TRAP positive cell number. (*** denotes $p < 0.001$ compared to the OVX group).

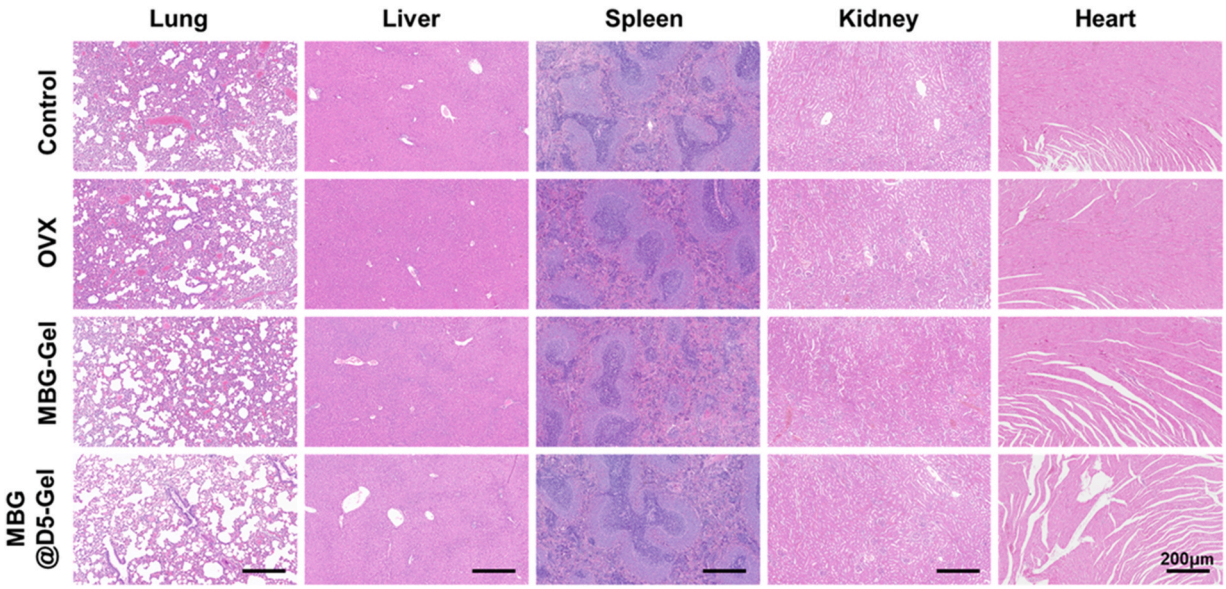

Fig. 7. Representative H&E stained images of kidneys, hearts, spleens, lungs, and livers in rats from each group.

bone formation during the healing of bone defects [25]. Xu Jiake and colleagues have identified three sequential stages in this process, based on the interaction and dominance of different cells: the initiation stage (dominated by osteoclasts), the reversal stage (where osteoclast activity is suppressed), and the termination stage (dominated by osteoblasts) [26]. In pathological conditions such as osteoporosis, this process is disrupted, making it difficult to sustain osteoclast suppression during the reversal stage and to activate osteoblasts during the termination stage [27,28]. Therefore, designing materials that can inhibit osteoclast activity during the reversal stage and promote osteoblast activity during the termination stage is crucial for the regeneration and repair of osteoporotic bone defects.

ALN, the most commonly used oral nitrogen-containing bisphosphonate, is effective in inhibiting bone resorption in osteoporosis. ALN has a high affinity for hydroxyapatite (HAp), which prevents its loss and inhibits osteoclast-mediated bone resorption. However, due to its polarity and hydrophilicity, ALN's oral absorption and bioavailability are limited, and oral or intravenous administration can cause severe side effects, highlighting the need for local drug delivery systems [29]. Hydrogels, which are highly hydrated, three-dimensional cross-linked networks formed by the aggregation of macromolecules, offer excellent swelling and shrinkage properties, and their injectability allows them to adapt to irregularly shaped sites. HAMA, as a typical macromolecule, exhibits excellent biocompatibility and degradability. HAMA, as a typical macromolecular material, exhibits good biocompatibility and degradability [30]. Additionally, photocurable hydrogels undergo gelation through liquid prepolymers under UV irradiation, and this externally induced gelation process endows the hydrogels with excellent plasticity [31]. In this study, we did not simply introduce ALN into the hydrogel system through mixing, but instead covalently grafted it onto the side chains of the macromolecules, thereby enhancing overall stability and effectively preventing the loss of ALN during the gel formation process.

To enhance the mechanical strength of the hydrogel, we introduced MBG material as an inorganic component to mimic the interactions between organic and inorganic components in bone tissue and modified the surface of MBG with a BMP-2 active peptide [32]. This peptide mimics the wristwatch region 30–34 sequence (DWIVA) of BMP-2 protein, binding to BMP receptor type I to promote osteogenic differentiation [12]. Using a mussel-inspired adhesion peptide strategy, the peptide is hydrogen-bonded to the MBG scaffold via catechol groups, achieving solid-liquid interface adsorption [33]. Mussels adhere to various substrates through special adhesive proteins (MAPs) on the surface of their byssus, and research by Waite et al. has shown that this adhesion mechanism is mediated by 3,4-dihydroxyphenylalanine (DOPA) [34]. Based on this theory, we grafted DOPA onto the DWIVA peptide to achieve hydrogen bonding with MBG. Compared to ALN, the degradation and release of DOPA are slower, which helps to promote osteoblast mineralization during the termination stage, sequentially synergizing with ALN to promote bone tissue regeneration.

In this study, we developed a novel multifunctional composite hydrogel system by combining HAMA with functionalized ALN and MBG nanoparticles loaded with bioactive peptides D5. This design integrates bone induction and bone resorption regulation, providing a promising solution for osteoporotic bone regeneration and repair. The incorporation of ALN into the HAMA matrix enhances the anti-resorptive capacity of the hydrogel, while the MBG nanoparticles, acting as carriers for D5, further contribute to osteoinduction through their controlled release properties. This dual-function approach overcomes the limitations of traditional single-function biomaterials, offering a more comprehensive therapeutic strategy for bone regeneration.

The hydrogel system demonstrated a sequential release of ALN and D5, which collectively targeted both osteoclast activity and osteoblast differentiation. In vitro drug release studies confirmed the hydrogel's ability to provide a sequential release profile, ensuring prolonged therapeutic effects at the defect site. This coordinated delivery mechanism represents an advancement in the design of drug-loaded biomaterials, matching the bone regeneration process under the pathologic microenvironment of osteoporosis.

MBG@D5-Gel exhibited excellent biocompatibility in both *in vitro* and *in vivo* analyses. When co-cultured with extracted BMMs, TRAP staining, bone resorption, and F-actin ring assays demonstrated that MBG@D5-Gel significantly inhibited osteoclast differentiation. RT-PCR and WB analyses further confirmed that the release of ALN inhibited osteoclast differentiation. To verify the effect of the peptides released by MBG@D5-Gel on osteogenic differentiation, we mixed it with osteogenic medium to prepare conditioned medium and cultured BMSCs in it. Alizarin red staining, ALP staining, as well as RT-PCR and WB results confirmed that the conditioned medium significantly promoted osteogenic differentiation.

In vitro studies showed that MBG@D5-Gel has dual effects in promoting osteogenesis and inhibiting bone resorption, making it a promising candidate for the treatment of osteoporotic bone defects. To further validate its *in vivo* efficacy, we conducted animal experiments to

evaluate its ability to promote the healing of osteoporotic bone defects. The OVX rat model is an ideal animal model for studying secondary osteoporosis, and the FDA has recommended it as the gold standard for modeling postmenopausal osteoporosis. In this study, a 2 mm diameter bone defect was created at the distal femur of SD rats, and MBG@D5-Gel was injected into the defect to observe its bone-forming ability. Micro-CT results showed that at 4 and 12 weeks post-surgery, only a small amount of new trabecular bone formed at the defect margins in the control and OVX groups, with an average proportion of less than 10 %, and trabecular bone loss was particularly pronounced in the OVX group. These results indicate poor autologous bone regeneration at the defect site under osteoporotic conditions. In contrast, the MBG-Gel and MBG@D5-Gel groups exhibited good bone formation effects, with the MBG@D5-Gel group showing significantly more new bone formation at 12 weeks than the MBG-Gel group, due to the later release of more D5 peptides promoting osteogenic differentiation. From a pharmacological perspective, the application of drug delivery systems in bone tissue engineering can reduce the toxic effects of high-dose burst release and prolong the drug's action time at the delivery site, thereby favoring osteogenesis. Numerous biomaterials have been shown to promote bone formation in osteoporotic bone defects. For example, the ALN scaffold developed by Wang Zhenxing et al. promoted the repair of osteoporotic bone defects [35]. Xu Youjia et al. proposed a dual-functional liposome strategy combining ALN with antiresorptive peptides, exhibiting excellent bone-targeting and bone resorption inhibitory effects [36]. However, these studies have overlooked the importance of the sequential effects of inhibiting osteoclast activity and promoting osteoblast differentiation in treating osteoporosis, which still requires further improvement. All in all, our work represents a preliminary attempt to regulate the timing of the bone remodeling process for the regeneration and repair of osteoporotic bone defects. The material design is well-conceived, and the results are promising.

5. Conclusion

In summary, in osteoporotic bone defect models, MBG@D5-Gel, as a sustained-release system, demonstrated the ability to sequentially release ALN and osteogenic active peptides, resulting in optimal promotion of bone regeneration. *In vivo* micro-CT reconstruction and histological staining confirmed that the OVX pathological microenvironment inhibits the regeneration and repair of bone defects. However, MBG@D5-Gel effectively inhibited bone loss and promoted the balance between bone formation and resorption in the osteoporotic bone defects of the OVX rat model. Although the specific mechanisms of inhibiting osteoclast activity and promoting osteogenesis require further investigation, the findings of this study suggest that MBG@D5-Gel is a promising biomaterial for effectively enhancing the osteogenesis process in osteoporotic bone defects.

CRediT authorship contribution statement

Lei Yu: Writing – original draft, Formal analysis, Data curation, Conceptualization. **Wentao Wang:** Formal analysis, Data curation, Conceptualization. **Chang Lv:** Data curation, Formal analysis, Methodology. **Qian Chen:** Methodology, Investigation, Formal analysis. **Peng Yang:** Software, Project administration. **Zhenrong Qi:** Resources, Methodology. **Haomiao Yu:** Software, Methodology. **Ruiqi Cao:** Software, Methodology. **Wenhao Li:** Software, Methodology. **Yi Qin:** Software, Methodology. **Gaoran Ge:** Software, Resources. **Peilai Liu:** Writing – review & editing, Validation, Funding acquisition. **Lixin Zhu:** Investigation, Supervision, Visualization, Writing – review & editing. **Houyi Sun:** Methodology, Formal analysis, Data curation, Writing – review & editing. **Dechun Geng:** Writing – review & editing, Supervision, Funding acquisition, Data curation, Conceptualization. **Liang Zhang:** Writing – review & editing, Visualization, Project administration, Funding acquisition.

Declaration of competing interest

The authors declare no conflict of interest.

Acknowledgements

This work was supported by the National Natural Science Foundation of China (82072425, 82072498, 82272567), the Natural Science Foundation project of Beijing Municipality (7222031), the Natural Science Foundation of Jiangsu Province (BK2021650), the Priority Academic Program Development of Jiangsu Higher Education Institutions (PAPD), Jiangsu Medical Research Project (ZD2022014), the Program of Suzhou Health Commission (GSWS2022002), National and Local Engineering Laboratory of New Functional Polymer Materials (SDGC2205), Foundation of National Center for Translational Medicine (Shanghai) SHU Branch (SUITM-202403), and the Project of MOE Key Laboratory of Geriatric Diseases and Immunology (No. KJS2502).

Appendix A. Supplementary data

Supplementary data to this article can be found online at https://doi.org/10.1016/j.mtbio.2025.101550.

Data availability

The authors do not have permission to share data.

References

[1] K.E. Ensrud, C.J. Crandall, Osteoporosis, Ann. Intern. Med. 177 (2024) ITC1–ITC16, https://doi.org/10.7326/AITC202401160.
[2] I. Foessl, H.P. Dimai, B. Obermayer-Pietsch, Long-term and sequential treatment for osteoporosis, Nat. Rev. Endocrinol. 19 (2023) 520–533, https://doi.org/10.1038/s41574-023-00866-9.
[3] J. Xu, L. Yu, F. Liu, L. Wan, Z. Deng, The effect of cytokines on osteoblasts and osteoclasts in bone remodeling in osteoporosis: a review, Front. Immunol. 14 (2023), https://doi.org/10.3389/fimmu.2023.1222129.
[4] Y. Cui, et al., Bone-targeted biomimetic nanogels Re-establish osteoblast/osteoclast balance to treat postmenopausal osteoporosis, Small 20 (2024) 2303494, https://doi.org/10.1002/smll.202303494.
[5] L. Autelitano, M.C. Meazzini, Alveolar cleft reconstruction with vomerine bone: two surgical procedures in one step: a case series, Plastic and Aesthetic Research 10 (2023) 16, https://doi.org/10.20517/2347-9264.2022.57.
[6] H. Guan, et al., Magnetic aggregation-induced bone-targeting nanocarrier with effects of Piezo1 activation and osteogenic–angiogenic coupling for osteoporotic bone repair, Adv. Mater. 36 (2024) 2312081, https://doi.org/10.1002/adma.202312081.
[7] C. Yan, et al., 3D-printed bone regeneration scaffolds modulate bone metabolic homeostasis through vascularization for osteoporotic bone defects, Biomaterials 311 (2024) 122699, https://doi.org/10.1016/j.biomaterials.2024.122699.
[8] D.M. Black, C.J. Rosen, Postmenopausal osteoporosis, N. Engl. J. Med. 374 (2016) 254–262, https://doi.org/10.1056/NEJMcp1513724.
[9] C. Ayers, et al., Effectiveness and safety of treatments to prevent fractures in people with low bone mass or primary osteoporosis: a living systematic review and network meta-analysis for the American college of physicians, Ann. Intern. Med. 176 (2023) 182–195, https://doi.org/10.7326/M22-0684.
[10] K.M. Hosny, Alendronate sodium as enteric coated solid lipid nanoparticles; preparation, optimization, and in vivo evaluation to enhance its oral bioavailability, PLoS One 11 (2016) e0154926, https://doi.org/10.1371/journal.pone.0154926.
[11] P.D. Papapetrou, Bisphosphonate-associated adverse events, Hormones (Basel) 8 (2009) 96–110, https://doi.org/10.14310/horm.2002.1226.
[12] L. Oliver-Cervelló, et al., An engineered biomimetic peptide regulates cell behavior by synergistic integrin and growth factor signaling, Adv. Healthcare Mater. 10 (2021) 2001757, https://doi.org/10.1002/adhm.202001757.
[13] Y. Zhao, et al., Multifunctional scaffold for osteoporotic pathophysiological microenvironment improvement and vascularized bone defect regeneration, Adv. Healthcare Mater. 12 (2023) 2203099, https://doi.org/10.1002/adhm.202203099.
[14] Y. Lei, et al., Functional biomaterials for osteoarthritis treatment: from research to application, Smart Med 1 (2022) e20220014, https://doi.org/10.1002/smmd.20220014.
[15] N. Oliva, J. Conde, K. Wang, N. Artzi, Designing hydrogels for on-demand therapy, Accounts of Chemical Research 50 (2017) 669–679, https://doi.org/10.1021/acs.accounts.6b00536.

[16] J. Kopeček, Hydrophilic biomaterials: from crosslinked and self-assembled hydrogels to polymer-drug conjugates and drug-free macromolecular therapeutics, J. Contr. Release 373 (2024) 1–22, https://doi.org/10.1016/j.jconrel.2024.05.012.
[17] W. Lu, et al., Human urine-derived stem cell exosomes delivered via injectable GelMA templated hydrogel accelerate bone regeneration, Materials Today Bio 19 (2023) 100569, https://doi.org/10.1016/j.mtbio.2023.100569.
[18] E. Anitua, L. Piñas, A. Murias, R. Prado, R. Tejero, Effects of calcium ions on titanium surfaces for bone regeneration, Colloids Surf. B Biointerfaces 130 (2015) 173–181, https://doi.org/10.1016/j.colsurfb.2015.04.006.
[19] A. Polo-Montalvo, et al., Effective actions of ion release from mesoporous bioactive glass and macrophage mediators on the differentiation of osteoprogenitor and endothelial progenitor cells, Pharmaceutics 13 (2021), https://doi.org/10.3390/pharmaceutics13081152.
[20] H. Yu, et al., Injectable PEG hydrogels with tissue-like viscoelasticity formed through reversible alendronate–calcium phosphate crosslinking for cell–material interactions, Adv. Healthcare Mater. 13 (2024) 2400472, https://doi.org/10.1002/adhm.202400472.
[21] J. Li, et al., MBG/PGA-PCL composite scaffolds provide highly tunable degradation and osteogenic features, Bioact. Mater. 15 (2022) 53–67, https://doi.org/10.1016/j.bioactmat.2021.11.034.
[22] W. Xia, J. Chang, Well-ordered mesoporous bioactive glasses (MBG): a promising bioactive drug delivery system, J. Contr. Release 110 (2006) 522–530, https://doi.org/10.1016/j.jconrel.2005.11.002.
[23] L. Wang, et al., Mechanical sensing protein PIEZO1 regulates bone homeostasis via osteoblast-osteoclast crosstalk, Nat. Commun. 11 (2020) 282, https://doi.org/10.1038/s41467-019-14146-6.
[24] Y. Wang, et al., A recombinant parathyroid hormone-related peptide locally applied in osteoporotic bone defect, Adv. Sci. 10 (2023) 2300516, https://doi.org/10.1002/advs.202300516.
[25] J.-W. Choi, Y.-C. Kim, Asian facial recontouring surgery. Plastic and Aesthetic Research 10 (2023) 59, https://doi.org/10.20517/2347-9264.2023.30.
[26] S. Zhu, et al., Coupling factors and exosomal packaging microRNAs involved in the regulation of bone remodelling, Biol. Rev. 93 (2018) 469–480, https://doi.org/10.1111/brv.12353.
[27] Y. Xu, et al., Electrospun fiber-based immune engineering in regenerative medicine, Smart Med 3 (2024) e20230034, https://doi.org/10.1002/smmd.20230034.
[28] S. Chen, et al., Catalpol attenuates osteoporosis in ovariectomized rats through promoting osteoclast apoptosis via the Sirt6-ERα-FasL axis, Phytomedicine 123 (2024) 155262, https://doi.org/10.1016/j.phymed.2023.155262.
[29] W.A. Camargo, J.W. Hoekstra, J.A. Jansen, J.J.J.P. van den Beucken, Influence of bisphosphonate treatment on bone substitute performance in osteoporotic conditions, Clin. Implant Dent. Relat. Res. 25 (2023) 490–501, https://doi.org/10.1111/cid.13203.
[30] M. Chen, et al., Injectable microgels with hybrid exosomes of chondrocyte-targeted FGF18 gene-editing and self-renewable lubrication for osteoarthritis therapy, Adv. Mater. 36 (2024) 2312559, https://doi.org/10.1002/adma.202312559.
[31] G. Eke, N. Mangir, N. Hasirci, S. MacNeil, V. Hasirci, Development of a UV crosslinked biodegradable hydrogel containing adipose derived stem cells to promote vascularization for skin wounds and tissue engineering, Biomaterials 129 (2017) 188–198, https://doi.org/10.1016/j.biomaterials.2017.03.021.
[32] R. Wu, et al., Injectable mesoporous bioactive glass/sodium alginate hydrogel loaded with melatonin for intervertebral disc regeneration, Materials Today Bio 22 (2023) 100731, https://doi.org/10.1016/j.mtbio.2023.100731.
[33] K.H. Park, K.-Y. Seong, S.Y. Yang, S. Seo, Advances in medical adhesives inspired by aquatic organisms' adhesion, Biomater. Res. 21 (2017) 16, https://doi.org/10.1186/s40824-017-0101-y.
[34] T. Wang, et al., Engineering immunomodulatory and osteoinductive implant surfaces via mussel adhesion-mediated ion coordination and molecular clicking, Nat. Commun. 13 (2022) 160, https://doi.org/10.1038/s41467-021-27816-1.
[35] Y. Zeng, et al., Sustained delivery of alendronate by engineered collagen scaffold for the repair of osteoporotic bone defects and resistance to bone loss, J. Biomed. Mater. Res. 108 (2020) 2460–2472, https://doi.org/10.1002/jbm.a.36997.
[36] J. Li, et al., Osteophilic and dual-regulated alendronate-gene lipoplexes for reversing bone loss, Small 19 (2023) 2303456, https://doi.org/10.1002/smll.202303456.